Vibration isolation system for cryocoolers of soft x-ray spectrometer on-board ASTRO-H (Hitomi)

Yoh Takei
Susumu Yasuda
Kosei Ishimura
Naoko Iwata
Atsushi Okamoto
Yoichi Sato
Mina Ogawa
Makoto Sawada
Taro Kawano
Shingo Obara
Chikara Natsukari
Atsushi Wada
Shinya Yamada
Ryuichi Fujimoto
Motohide Kokubun
Noriko Y. Yamasaki
Hiroyuki Sugita
Kenji Minesugi

Yasuo Nakamura
Kazuhisa Mitsuda
Tadayuki Takahashi
Seiji Yoshida
Shoji Tsunematsu
Kenichi Kanao
Katsuhiro Narasaki
Kiyomi Otsuka
F. Scott Porter
Caroline A. Kilbourne
Meng P. Chiao
Megan E. Eckart
Gary A. Sneiderman
James T. Pontius
Dan McCammon
Paul Wilke
John Basile

Vibration isolation system for cryocoolers of soft x-ray spectrometer on-board ASTRO-H (Hitomi)

Yoh Takei,[a,b,][*] Susumu Yasuda,[b] Kosei Ishimura,[a] Naoko Iwata,[a,b] Atsushi Okamoto,[b] Yoichi Sato,[b] Mina Ogawa,[a] Makoto Sawada,[c] Taro Kawano,[a,b] Shingo Obara,[b] Chikara Natsukari,[a] Atsushi Wada,[a] Shinya Yamada,[d] Ryuichi Fujimoto,[e] Motohide Kokubun,[a] Noriko Y. Yamasaki,[a] Hiroyuki Sugita,[b] Kenji Minesugi,[a] Yasuo Nakamura,[a] Kazuhisa Mitsuda,[a] Tadayuki Takahashi,[a] Seiji Yoshida,[f] Shoji Tsunematsu,[f] Kenichi Kanao,[f] Katsuhiro Narasaki,[f] Kiyomi Otsuka,[f] F. Scott Porter,[g] Caroline A. Kilbourne,[g] Meng P. Chiao,[g] Megan E. Eckart,[g] Gary A. Sneiderman,[g] James T. Pontius,[g] Dan McCammon,[h] Paul Wilke,[i] and John Basile[i]

[a]Japan Aerospace Exploration Agency, Institute of Space and Astronautical Science, Chuo-ku, Sagamihara, Kanagawa, Japan
[b]Japan Aerospace Exploration Agency, Research and Development Directorate, Tsukuba, Ibaraki, Japan
[c]Aoyama Gakuin University, Department of Physics and Mathematics, Chuo-ku, Sagamihara, Kanagawa, Japan
[d]Tokyo Metropolitan University, Department of Physics, Hachioji, Tokyo, Japan
[e]Kanazawa University, Faculty of Mathematics and Physics, Kakuma-machi, Kanazawa, Ishikawa, Japan
[f]Sumitomo Heavy Industries, Ltd., Industrial Equipment Division, Niihama, Ehime, Japan
[g]NASA/Goddard Space Flight Center, Greenbelt, Maryland, United States
[h]University of Wisconsin, Department of Physics, Madison, Wisconsin, United States
[i]Moog CSA Engineering, Mountain View, California, United States

Abstract. The soft x-ray spectrometer (SXS) onboard ASTRO-H (named Hitomi after launch) is a microcalorimeter-type spectrometer, installed in a dewar to be cooled at 50 mK. The energy resolution of the SXS engineering model suffered from microvibration from cryocoolers mounted on the dewar. This is mitigated for the flight model (FM) by introducing vibration isolation systems between the cryocoolers and the dewar. The detector performance of the FM was verified before launch of the spacecraft in both ambient condition and thermal-vacuum condition, showing no detectable degradation in energy resolution. The in-orbit detector spectral performance and cryocooler cooling performance were also consistent with that on ground, indicating that the cryocoolers were not damaged by launch environment. The design and performance of the vibration isolation system along with the mechanism of how the microvibration could degrade the cryogenic detector is shown. Lessons learned from the development to mitigate unexpected issues are also described. © The Authors. Published by SPIE under a Creative Commons Attribution 3.0 Unported License. Distribution or reproduction of this work in whole or in part requires full attribution of the original publication, including its DOI. [DOI: 10.1117/1.JATIS.4.1.011216]

1 Introduction

The soft x-ray spectrometer (SXS)[1] onboard an x-ray astronomy satellite ASTRO-H[2] is a cryogenic microcalorimeter-type spectrometer operating at 50 mK. The detector consists of 6×6 pixels, covering the field-of-view of $3' \times 3'$ in combination with a soft x-ray telescope.[3] The key characteristic of SXS is a superb spectroscopic performance: requirement of 7 eV (full-width half-maximum) at 6 keV. SXS is a thermometer-based detector, detecting an x-ray photon as a heat input; every time the detector pixel absorbs an x-ray photon, the pixel temperature increases by an amount corresponding to incident x-ray energy and then recovers to the original temperature with a ∼ms time constant. The detector heat sink temperature needs to be low (∼50 mK) and stable ($\leq 2.5~\mu K_{rms}$) in order to achieve the required energy resolution.

SXS is, by its nature as a microcalorimeter (i.e., thermometer), sensitive to not only x-ray photons but also any energy input. Stray energy input could increase the noise of the detector and/or cause gain variation, both of which could significantly degrade the energy resolution. Microvibration, or disturbance, is one of the potential stray energy sources. Indeed, the energy resolution of the SXS engineering model (EM) suffered from disturbance from cryocoolers. The temperature stability requirement was not satisfied when the cryocoolers were in operation, resulting in unacceptable degradation in energy resolution. This issue demanded the unplanned design change of the flight model (FM) dewar. Vibration isolation systems, consisting of isolators (springs and viscoelastic materials; VEM), thermal straps, and bumpers were introduced to the FM dewar, in order to mechanically isolate the cryocooler vibration from the dewar. The vibration isolation system successfully recovered the energy resolution of the FM SXS. No degradation was measured when cryocoolers were in operation.

Because of low-noise and high-sensitivity characteristics of cryogenic detectors (microcalorimeters and bolometers), future astronomy missions in various wavelengths plan to utilize a cryogenic detector, including Athena X-IFU[4] (x-ray), SPICA SAFARI[5] (infrared), and LiteBIRD[6] (microwave). This paper provides insights on the mechanical vibration issue and a counter measure including lessons learned during the SXS developments, which would be informative or applicable in the development of future cryogenic detectors.

---

*Address all correspondence to: Yoh Takei, E-mail: takei.yoh@jaxa.jp

The organization of this paper is as follows: Sec. 2 describes the overview of the SXS cooling system, Sec. 3 describes the details of the disturbance issue observed with the SXS EM, Sec. 4 describes the mitigation applied, Sec. 5 describes the resulting FM performance, and Sec. 6 describes lessons learned as a conclusion.

2 Overview of the SXS Cooling System

The SXS detector is located inside a dewar with dimensions of 1.8 m in height and 1.4 m in diameter. The illustration of the dewar is shown in Fig. 1. The detector is cooled by a hybrid cooling system consisting of mechanical cryocoolers, superfluid helium contained in a He tank, and a three-stage adiabatic demagnetization refrigerator (ADR).[7,8] The cryocoolers used were four sets of two-stage Stirling coolers (2ST) and a Joule–Thomson (JT) cooler. There are four vapor cooled shields (VCS) inside the dewar: outer VCS (OVCS), middle VCS, inner

VCS (IVCS), and JT cooler shield (JTS). Two of the 2ST (called SC-A and SC-B) are used to cool OVCS (to <150 K) and IVCS (to <30K), while the other two 2STs (PC-A and PC-B) are used to precool the JT pluming to achieve the JTS temperature of <4.5 K by the JT effect. Maintaining a low vapor pressure keeps the He tank temperature at <1.3 K, and therefore in the superfluid state. The ADR cools the detector down to 50 mK.

A schematic of dewar mechanical structure is shown in Fig. 2(a). The inner structure of the dewar utilizes a suspension mechanism to minimize the conductive heat load. The IVCS is suspended from the dewar main shell (DMS) by glass fiber-reinforced plastic straps, the He tank is suspended from IVCS by carbon fiber-reinforced plastic straps, and the detector and its heat sink (calorimeter thermal sink; CTS) is suspended by Kevlar strings [see Fig. 2(b)].[7] A 2ST consists of a compressor, a cold head, and a capillary tube connecting the compressor and
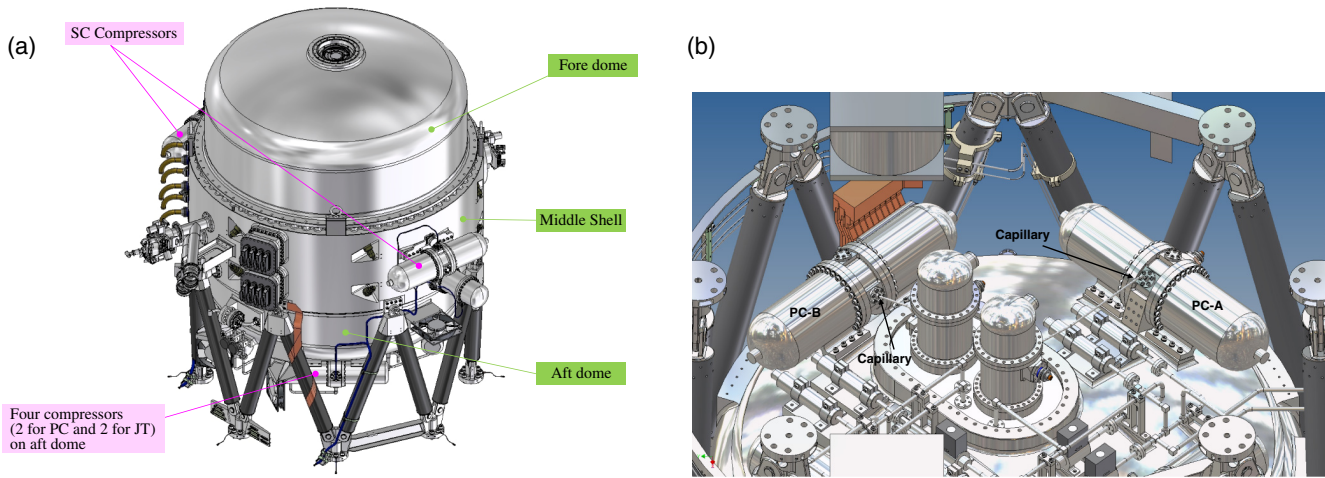

Fig. 1 Illustration of the SXS dewar: (a) front view and (b) bottom view.
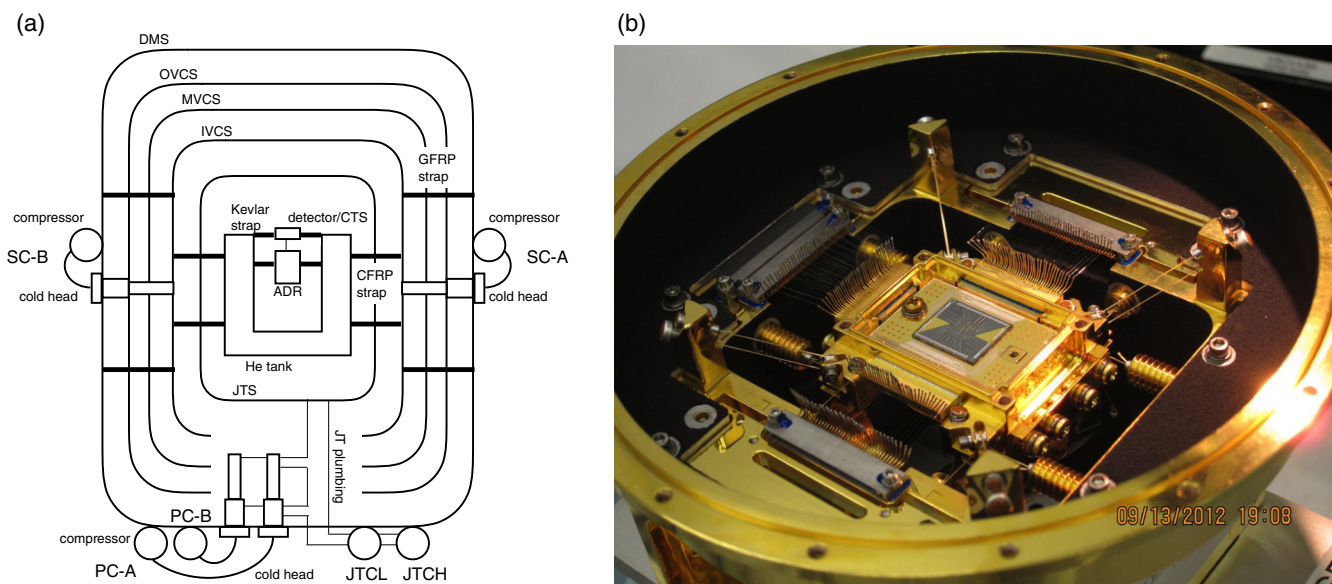

Fig. 2 (a) Schematic of the mechanical structure of the dewar. (b) Photo of SXS FM detector.[9,10] The size of the 6 × 6 detector array in the center is 5 mm × 5 mm. The inner structure is CTS, suspended by Kevlar wires; the Kevlar wires are seen at the corner of CTS.

the cold head. A JT consists of two compressors (JTCL for lower pressure and JTCH for higher pressure) and plumbings. Both the 2STs and the JT are mounted on the outer surface of DMS.[7,11]

When the cryocoolers are in operation, the compressors and cold heads warm up because of the electrical power applied. The dissipated heat is transported to either the dewar surface or radiator panels and radiated to deep space. Loop heat pipes (LHPs) are used for heat transfer from each SC-A/B compressor and cold head to a spacecraft cold plate, while thermal straps are used from PC-B and JTCL compressors to spacecraft cold plates. Heat from the PC-A compressor, PC-A/B cold heads, and JTCH compressor is conducted only on the dewar surface.[12]

3 Vibration of Cryocoolers Degrading the Energy Resolution

3.1 Observed Influence of Cryocooler Vibration

During the performance test of the EM SXS, the energy resolution of the detector was found to be degraded when cryocoolers were in operation. The influence of cryocoolers was identified in three ways: change of temperature of the detector heat sink (CTS) and its fluctuation, increase of detector noise, and degradation of the detector energy resolution.

Figure 3(a) shows the CTS temperature of the EM SXS as a function of time. The temperature and its fluctuation in standard deviation (hereafter σ_T) increased when one of the cryocoolers was on. While σ_T satisfied the requirement of <2.5 μK_{rms} when the cryocoolers are off, it degraded to up to ~40 μK_{rms}, depending on cooler power. An increase of low frequency (particularly in ≲30 Hz) noise was also observed in a noise spectrum, a Fourier-transformed electrical signal from the detector taken when no x-ray is detected (an example of the noise spectrum of FM sensor is shown in Fig. 7). This is understood as a result of low-frequency fluctuation of the detector temperature, corresponding to the fluctuation of the CTS temperature.

Figure 3(b) shows the relation between the energy resolution of a detector pixel and σ_T measured with the EM SXS. When σ_T is large, the energy resolution is degraded to ~50 eV in some cases, while the requirement of the energy resolution is 7 eV. On the other hand, the "baseline resolution" (not shown on the plot), which is the width of the energy histogram made through the same signal processing as for x-rays when there is no x-ray

hitting the pixel, degrades by only ~2 eV, even when σ_T is 44 μK_{rms}. This indicates that the degradation of energy resolution was primarily due to the gain variation in lower frequency (i.e., slower) than the detector of the signal band, while the contribution of in-band noise was small. The gain variation is attributed to CTS temperature fluctuations, due to the vibration heating, given that the response (gain) of the SXS detector is temperature dependent. The observed increase of heat load on the CTS is on the order of 10 nW. Also note that is is confirmed that the CTS temperature, not only thermometer reading, actually fluctuates.

The degradation always occurs when the cryocoolers are on, while the degree of degradation is quantitatively not highly reproducible; small change in the dewar configuration or in cryocooler operation affects the degradation. It turns out that the vibration of 2ST compressors is the primary origin of the degradation, while the JT compressors and 2ST cold heads make little influence (how it is understood is shown in Sec. 3.2).

3.2 Mechanism of How Energy Resolution was Degraded

The frequencies to which the CTS temperature was sensitive were investigated by applying single-frequency sine vibration on the dewar outer surface and sweeping the frequency, using an electromagnetic shaker. The sensitivity depends on both the transmissibility of the dewar structure and the stimulation efficiency at CTS. It was not uniform; the CTS temperature changes, abruptly, only at some (10 to 20, depending on the direction of vibration) frequencies between 140 and 600 Hz, while the sensitivity below 100 Hz is low. The sensitive frequencies are sparsely distributed, and each of them is extremely sharp; sensitive range is ~1 Hz. Given the frequencies and sparse and sharp characteristics, the sensitive frequencies likely correspond to resonances at vibration modes of CTS or ADR. The temperature increase, and hence, the degradation of detector performance, only occurs when the input vibration has power at these sensitive frequencies, to excite resonance vibration.

The vibration force spectra of cryocoolers were also measured. Both the spectra of 2ST and JT show the line features at the driving frequency (15 Hz for 2ST and 52 Hz for JT) and its harmonics. In addition, the spectrum of the 2ST compressor contains a continuum feature above ~200 Hz, caused by frictional motion, of the level of ~2 N_{rms} integrated in 0 to
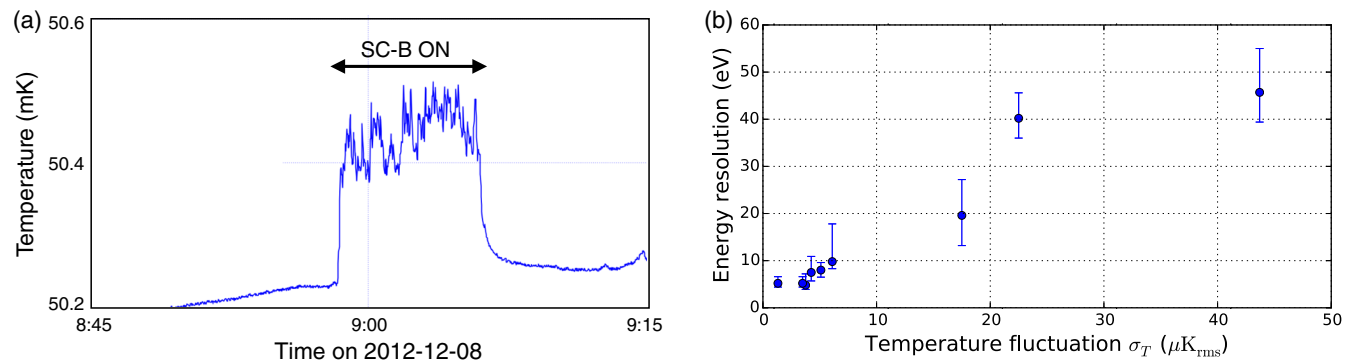
Fig. 3 (a) Temperature of CTS as a function of time measured with the EM SXS. The temperature control by ADR is in open-loop during this measurement. The temperature and its fluctuation is larger when SC-B is on, compared to other duration in which all cryocoolers are off. (b) Relation between the energy resolution of the detector pixel and CTS temperature fluctuation measured with the EM SXS. Each data point corresponds to a different cryocooler power.

500 Hz for each axis.[11] The vibrational heating occurs because of the coincidence of vibration spectrum and the sensitive frequency.

One of the important characteristics of this vibration issue is a strong nonlinear response. When the vibration level is increased, the resultant temperature change is larger than proportional. Also, since the dewar shell has several vibration modes at $\gtrsim 300$ Hz, the transmissibility of the vibration from the dewar surface to the CTS depends on the location of vibration source (i.e., location of cryocoolers). It was observed that σ_T changed when other structures were attached on the dewar, probably because of the vibration mode(s) being altered.

Since the number of sensitive frequencies is limited and since each sensitive frequency is sharp, harmonics of driving frequency of cryocoolers can be set away from the sensitive frequencies, by small adjustment of the driving frequency within the capability of cryocoolers and its drivers. With this adjustment, the only remaining heating source was the continuum in the vibration spectrum of the 2ST compressors. When the compressor was temporarily detached from the dewar and supported by another structure, the heating diminished. It confirms that the contribution of the JT compressors and 2ST cold heads, whose vibration spectrum contains only line features, is negligible.

It should be noted that the electrical pick-up noise observed as line noise in the noise spectrum makes negligible contribution on the energy resolution because they appear in higher frequencies than those the detector is sensitive. The "microphonics" noise, i.e., the electrical noise induced by vibration of wires, is hence not the origin of performance degradation.

In summary, the mechanism of how cryocooler mechanical disturbance degraded the SXS detector energy resolution can be described as follows. The continuum vibration of 2STs in the frequency of several hundred hertz was transmitted to the interior of the dewar, stimulating the resonance vibration of the detector cold stage, and then inducing a variable heat input to the detector heat sink. This variation in heat load caused significant gain variation of the detector, resulting in unacceptable degradation in energy resolution. It should be noted that the frequency of temperature fluctuation is not the same as the frequency of the vibration that induced the temperature fluctuation, because the variation of the temperature is determined by average heat input over the thermal time constant. Actually the former is mainly <1 Hz, while the latter is >200 Hz. Also if the (averaged) heat input had not fluctuated but was constant over time, the temperature stability would not be degraded. The actual heat input by vibration was, however, stochastic.

4 Vibration Isolation System

4.1 Required Functions for the Vibration Isolation System

The vibration isolation system (hereafter VIS) was introduced to the FM SXS dewar for mitigation of the cryocooler disturbance; four sets of VIS were inserted between the dewar and each 2ST compressor. A VIS that incorporates springs reduces the transmission of vibration at high frequency. With a linear 1 degree of freedom (DoF) spring and damper, the transmissibility of the force $T(f)$, i.e., the ratio between the force at the mounted interface to the force produced by a compressor, is expressed as follows:

$$T(f) = \sqrt{\frac{1 + (2\zeta\kappa)^2}{(1 - \kappa^2)^2 + (2\zeta\kappa)^2}}, \qquad (1)$$

where ζ is a damping ratio to the critical damping, and $\kappa = f/f_0$ is a ratio of the frequency and the natural frequency of the spring f_0. This equation gives $T(f) < 1$ when $\kappa > \sqrt{2}$. Since vibration heating is mainly due to the vibration at >200 Hz while the sensitivity for vibration below 100 Hz is low, springs with natural frequencies below 100 Hz can be a good vibration isolation system. Note that six DoF (three in translation and three in rotation) needs to be considered for designing the isolators. Preferable sets of f_0 and ζ are $f_0 < 100$ Hz and $\zeta \gtrsim 0.01$, in the six fundamental modes, and no surge (local) modes below 600 Hz.

Other mitigations—such as inserting rubber dampers, changing inner-dewar structure to reduce transmissibility or sensitivity, improving compressor design to reduce the generated vibration, and relocating the compressor to other places than dewar surface—had also been investigated but were not adopted. It is concluded that they were not feasible either because the expected improvement would not be enough or because required modification would be too much considering the stage of the development.

The required function of the VIS is not only (1) the reduction of vibration transmissibility but also (2) thermal conductivity between the compressor and the dewar; (3) moderate (allowable) vibration amplification, and displacement under mechanical load of launch and ground testing. Another important requirement is (4) mechanical interface to avoid redesign of the dewar.

The reduction of transmissibility (requirement 1) must be considered not only in a single DoF but in six DoF and as a function of frequency. Since the dependence is complex, the quantitative requirement of the transmissibility cannot be reliably determined by analysis alone. Therefore, the requirement was determined experimentally, by measuring the temperature change when various vibrations were applied at the location of the SC-B compressor by a shaker system with six electromagnetic shakers, which can apply arbitrary 6-DoF force.[13] The transmissibility requirement must be satisfied in any possible temperature in orbit, between $-27°C$ and $+34°C$. The details of derivation and the resultant level are presented Ref. 13.

Since the insertion of a VIS decouples the thermal connection between the compressor and the dewar, a thermal link must be added (requirement 2). The required thermal conductance is 2.0 W K^{-1} for SC-A, SC-B, and PC-A. The thermal link for the PC-B compressor is connected not to the dewar but to the spacecraft cold plate that is thermally connected to the spacecraft radiator with heat pipes. The required thermal conductance is 1.0 W K^{-1}. The thermal links must be flexible in order to keep the vibration transmissibility small enough (requirement 1).

Another requirement is to keep the acceleration and displacement at the compressor within the allowable level when low-frequency (<100 Hz) mechanical load is applied to the spacecraft during ground testing or during launch (requirement 3). The vibration at the dewar is amplified at the compressor by a VIS around its natural frequencies. The acceleration must not cause excessive mechanical load to the inner-compressor components. In addition, the relative displacement between the compressor and the dewar must be small enough since otherwise the capillary tube connecting a 2ST compressor and a cold head could be damaged. The pogo oscillation of the second stage

burning of the launch vehicle (H-IIA rocket) around 30 to 40 Hz needs special care.

Finally, the VIS must be designed so that it can be inserted and mounted without significant redesign of the dewar (requirement 4), because the FM SXS dewar had been already in fabrication when introduction of the VIS was determined. The available bolt interface to mount the VIS is only existing ones. The available interval between the dewar surface and compressor bottom plate is 35 mm. The dynamic envelope of VIS must not cause any mechanical interference to the existing dewar structure. This requirement turned out to be a significant constraint on the VIS design.

In addition to these function requirements, the VIS must be compliant with space environment (vacuum, extreme temperature, radiation, atomic oxygen, and ultraviolet light), spacecraft requirement (such as low outgassing), and with launch and ground-testing environment (mechanical load). The function must be retained for longer than the lifetime of the spacecraft, 3 years.

It should be emphasized that the four requirements somewhat conflict with each other. A stiff thermal link would be good for better thermal conductance, but it would violate the transmissibility requirement. A spring of low natural frequency would be good to reduce the transmissibility in high frequency, but it would generate too large a displacement. Because of the limited available space, a launch lock mechanism, which was once thought an option for requirement 3, was abandoned in the early phase of a trade study.

4.2 Design of the Vibration Isolation System

The VIS was designed and fabricated by MOOG CSA,[14] utilizing their SoftRide technology.[15] SoftRide is a flexure spring combined with VEM for damping. Graphite fiber thermal straps (GFTS™) from TAI Inc. was adopted for the thermal link because of its flexibility. In addition, bumpers are used to restrict the excessive motion and when launch and ground-testing vibration is applied. These three, namely SoftRide isolators, GFTS thermal links and bumpers, are the key components of the SXS VIS. The materials that had been used in space are selected in order to ensure the space-environment compatibility.

A schematic of the VIS is shown in Fig. 4. Components that are from the original dewar design are shown in blue, while those of the VIS is shown in brown and black. Two plates (dewar plate and compressor plate) are added and connected to each other by four SoftRide isolators (flexure springs with VEM). Four bumpers are attached on each VIS. A bumper consists of a pin and a sleeve. The pin is attached to the compressor plate, while the sleeve, along with associated VEM, is attached to the dewar plate. The pin and sleeve are not in contact when no vibration is applied, while they hit each other to restrict relative displacement when vibration is applied. GFTS thermal link thermally connects the compressor and the dewar for SC-A, SC-B, and PC-A, and connects the compressor and spacecraft cold plate for PC-B.

For designing and development, both the software-based analysis using finite-element models (FEMs) and hardware-based testing using engineering development units (EDU) were utilized. First, the iteration in designing the VIS was performed using the FEM until the desired mechanical and thermal properties were obtained. Two EDU units were then constructed. The EDUs were tested to verify the performance and to verify the FEM. The design of flight hardwares was decided reflecting the test results and lessons learned with EDU. Fortunately, only small modification from EDU was required. Finally flight hardwares were fabricated, tested, and delivered. Since EDUs have sufficient fidelity to the flight units, they were used as representatives of flight units whenever additional tests for further characterization were demanded.

Figure 5 shows the photos of VIS at SC-B, PC-A, and PC-B mounted on the dewar. The VIS of SC-A and SC-B has the identical design in bilateral symmetry, while the design is slightly different between SC, PC-A, and PC-B ones. Four flexure isolators are located at the sides of each compressor. Four bumpers are located at the four corners of each compressor. The bumper structure is not visible because it is hidden under a bumper cap. Seven GFTS units are used for each of SC-A, SC-B, and PC-A VIS. Two of them are at the sides of the compressor, between the two flexures. GFTS of PC-B VIS has a completely different design from the others, because an end of PC-B GFTS is connected to the spacecraft cold plate, not the dewar, as shown in
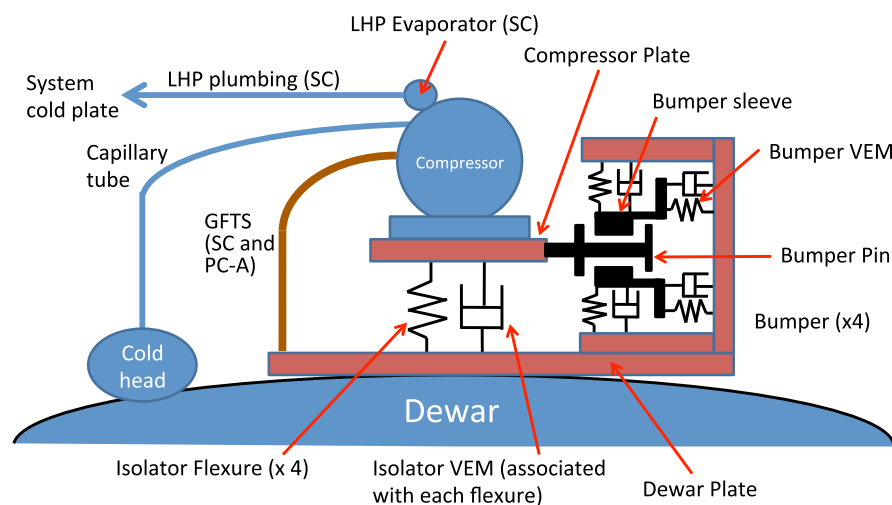
Fig. 4 Schematic of the VIS. Components that are from the original dewar design are shown in blue, while constituents of the VIS are shown in brown and black. The GFTS on PC-B is connected directly from the compressor to the spacecraft cold plate.
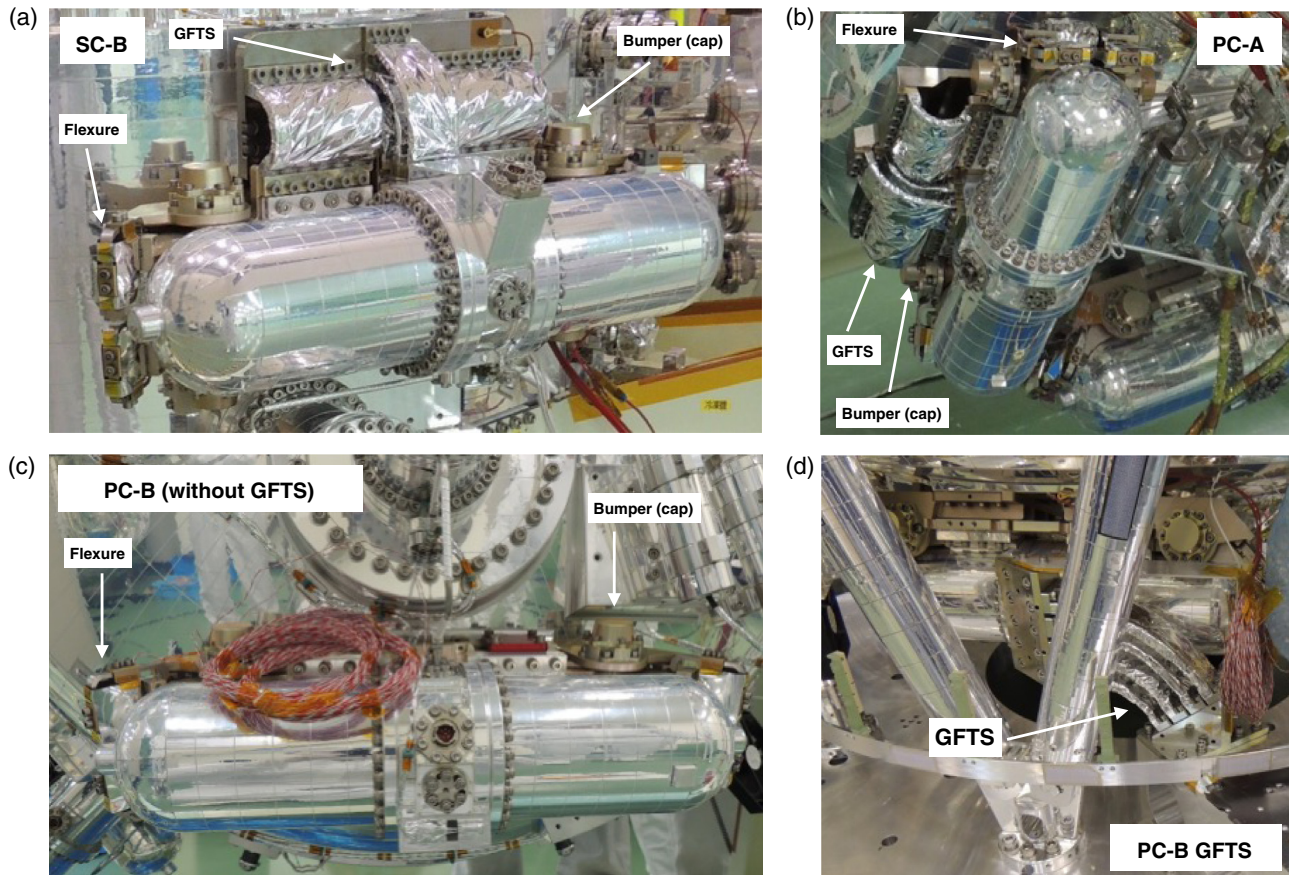
Fig. 5 VIS photos mounted on the dewar: (a) SC-B, (b) PC-A, (c) PC-B before GFTS installation, and (d) PC-B GFTS. Note that the dewar was not in the final configuration since some flight components were not installed at the time. Photo of SC-A is not shown because the VIS of SC-A and SC-B are in bilateral symmetry.

Fig. 5(d). It consists of four bigger GFTS units. Since GFTS is covered by an aluminized mylar, the graphite part is not visible. The shape and routing of LHP plumbings for SC-A and SC-B compressors and capillary tubes for each 2ST was modified from the EM SXS dewar to fit the new location of compressors.

4.3 Verification of Mechanical Response of the VIS

Since the requirements were mutually conflicting and hence challenging, the measurement and verification of the VIS mechanical response was crucial. The dynamic stiffness and damping of the VEM and GFTS were measured, along with their temperature dependence. The VEM whose stiffness had too large temperature dependence was not adopted. The stiffness of GFTS turned out to be much larger at $\sim -20^{\circ}C$ than at room temperature (more than one order of magnitude, for some test sample). These measured properties were included in FEMs to calculate the transmissibility including higher-order modes.

Estimating response against (large) vibration during launch and ground-testing was even more challenging. Since the stiffness and damping of the bumper exhibits a sharp change when the bumper pin and sleeve start to touch each other, response of the bumpers is amplitude dependent and nonlinear, making standard analysis in the frequency domain not applicable. As illustrated in Fig. 4, stiffness and damping increase when the bumper touches. This behavior was represented by a hardening-type bilinear spring. The response during launch and ground-testing

was then calculated by nonlinear analyses in the time domain, using 6 DoF time-domain acceleration sequence at the dewar (mount point of an isolator) as input to obtain time-domain acceleration and displacement at the compressor as output. The rotative motion of the compressor was considered in calculation. From this time-domain output, the maximum acceleration on the compressor and the maximum stress on the capillary tube were derived.

The input time-domain acceleration data for launch environment were calculated based on the coupled-load analysis (CLA), in which the structural math models of a spacecraft, including the dewar, and that of a rocket are combined to calculate the transient acceleration during launch. The nonlinear bumper response was not included in the CLA, because the CLA is a linear analysis and the bumper response affects the response of the heavy dewar and spacecraft very little. Multiple input sequences were calculated so that uncertainties of the math model and launch environment are taken into account.

The analyses described above were compared to the measurement, i.e., response of the VIS EDU. The measured response was larger than the analysis in some cases, although the analyses reproduced the complex VIS response reasonably well in most cases. To make sure that the maximum possible acceleration and displacement are within the allowable range, extensive tests were performed using the EDU with a hydraulic simulation table capable of applying arbitrary 6 DoF vibration input. The test was performed for three configurations (SC-A/B,
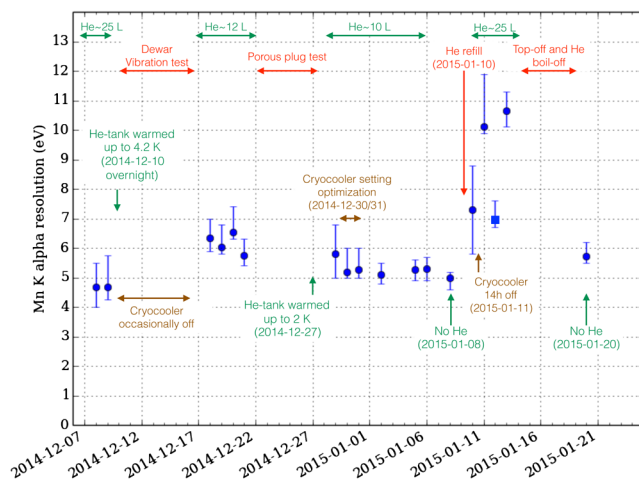
PC-A, and PC-B), for four temperatures (5°C, 10°C, 15°C, and 25°C), for two bumper shifts caused by static acceleration during launch (corresponding to 1.0 G and 2.5 G), and for two input levels (typical CLA out level and ×1.2). The input sequence includes multiple CLA patterns covering uncertainties of CLA. For each test case, three vibration runs were applied to check the reproducibility. In total, 126 vibration runs were performed. Not until finishing this extensive test campaign was the VIS finally decided to be adopted as a solution to the disturbance issue. The details of the test verification of the VIS can be found elsewhere.[15] It was also learned from the test that the acceleration can be unacceptably large in some cases at 5°C, leading to adding the requirement on the temperature during launch: 10–25°C at compressors and the dewar.

5 Performance of the SXS Flight Model

5.1 Performance Without VIS

Various verification and measurements were performed with the SXS FM, before the VIS was installed. The energy resolution taken during this period is shown in Fig. 6. As noticed in Fig. 6, the energy resolution was not stable. It satisfied the requirement at some measurements, but not always. The temperature fluctuation showed clear correlation with the temperature fluctuation. Unstable energy resolution and temperature fluctuation suggest that the heat load to the CTS was not constant due to unknown or uncontrolled differences.

The measurement condition during this period was not exactly the same. The amount of He varied by time. The cryocooler setting was changed. Verification tests besides the energy resolution measurement were performed, such as a vibration test and a porous plug performance test. There is, however, no single parameter showing clear correlation with the energy resolution, although it seems that the smaller amount of He leads to better energy resolution after (and only after) December 17, 2014, i.e., the vibration test. Provided the sharp frequency dependence of the heat load or more than proportional dependence on the vibration (see Sec. 3.2), it would be probable that a subtle change of configuration results in a significant change in energy resolution.

With such an uncertainty, it is difficult to accurately predict the energy resolution after the configuration further changes, e.g., after the dewar is integrated to spacecraft or after the spacecraft is in orbit. Therefore, once vibration heating is observed with a microcalorimeter instrument of a future mission, in-orbit performance needs to be carefully evaluated since the energy resolution requirement could be violated even if the requirement is satisfied at on-ground measurement.
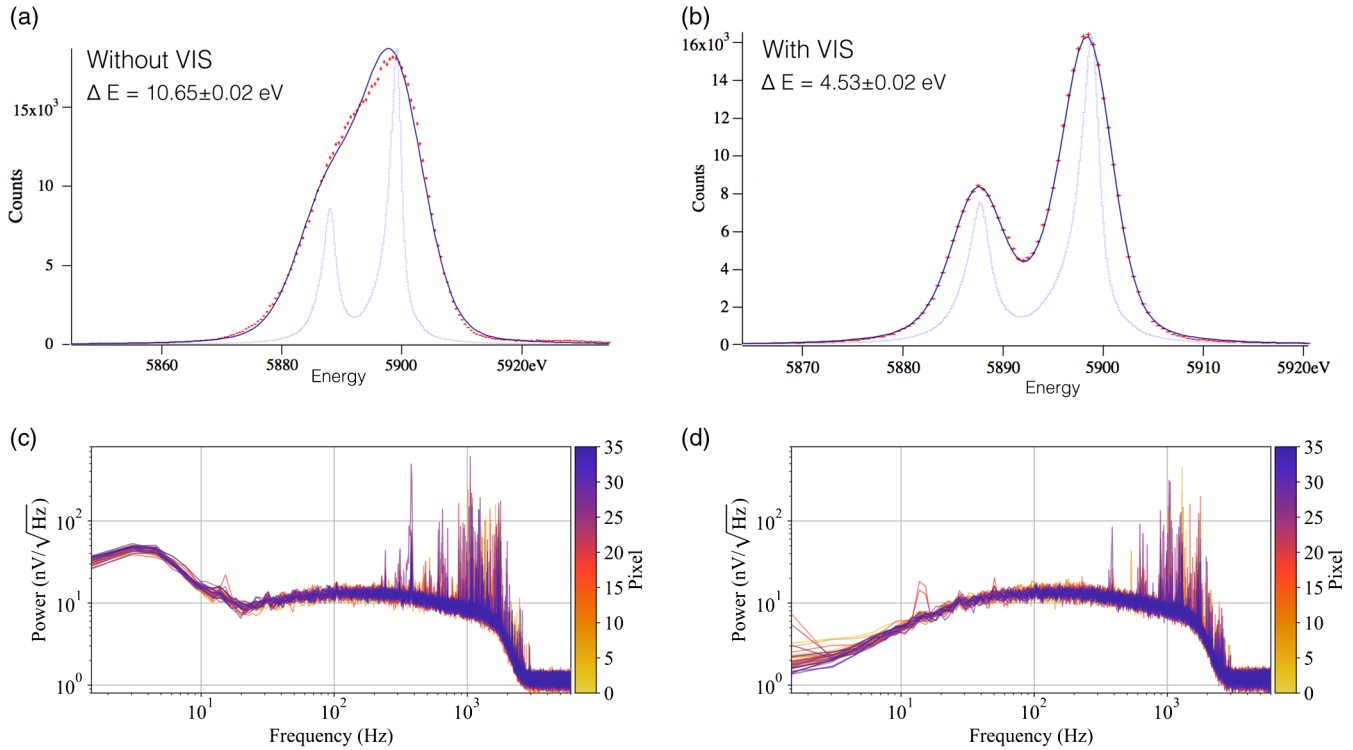
5.2 Performance with VIS

The energy histogram of Mn Kα emission lines at 5.9 keV from all detector pixels combined with the FM SXS detector is shown in Figs. 7(a) and 7(b). The noise spectra are shown in the bottom panels (c and d). Data taken during ground testing before the dewar was installed on the spacecraft are shown compared. Left panels (a and c) show those without VIS, while right panels (b and d) with VIS.

Energy resolution was significantly improved. Indeed, the energy resolution with the VIS was consistent with that taken with the cryocooler turned-off. From the noise spectra shown in the bottom panels (c and d), it is clear that the low-frequency bump in the noise spectra without VIS diminished after VIS installation. The line noises in high frequency (>100 Hz), seen in both plots, are due to electrical interfaces mainly by cooler-drive electronics. Since they are out of the detector signal band, energy resolution of the detector is not affected by them.[16]

Temperature fluctuation σ_T was also improved from ∼4 to ∼0.5 μK_{rms}. Note that the temperature fluctuation without VIS is smaller than that of the EM SXS, although still not enough to satisfy the requirement, as a result of a larger thermal conductance between the detector and the ADR; the conductance of the FM SXS is larger than the EM SXS by a factor of 8. The effect of the VIS can also be seen in the acceleration spectrum measured on the DMS, as shown in Fig. 8. By installation of the VIS, the continuum spectrum in acceleration above 200 Hz was reduced by a factor of ∼10. The lines seen in all data shown in Fig. 8 correspond to the driving frequencies and their harmonics of cryocoolers. Since the JT compressors and 2ST cold heads are directly attached on the DMS (note that the VIS are applied to only 2ST compressors), the vibration at these harmonics is still conducted to the dewar. Because these frequencies are not aligned to the resonance frequencies of CTS, the vibration does not impose heat or temperature fluctuation to CTS.

The acceleration spectrum stays small after the dewar is mounted to the spacecraft, although it varied a little. The acceleration did not exhibit long-term change, as seen by orange (taken on May 11, 2015) and brown (taken on November 13, 2015) curves of Fig. 8.

The performance of the SXS did not change after various spacecraft tests, such as electrical function test, thermal-vacuum test, and mechanical environment test. In the thermal-vacuum test, the detector performance (i.e., transmissibility of the VIS) in the orbit-like temperature was verified. The thermal conductance of the VIS and GFTS, measured before the VIS was mounted on the dewar, was measured as 2.10, 2.16, 2.00, and 1.18 W K^{-1} for SC-A, SC-B, PC-A, and PC-B, respectively. The end-to-end thermal performance was verified in the thermal-vacuum test.[17]

Fig. 6 History of the energy resolution at 5.9 keV (Mn Kα line) of SXS FM before installation of the VIS, taken from December 2014 to January 2015. The error bars indicate variation among pixels. The data shown as a square mark on January 12, 2015 was taken with different calorimeter bias. Amount of He, activities on the dewar, and cryocoolers are also indicated.

(a)

(b)

(c)

(d)

Fig. 7 Energy histogram of Mn Kα emission lines at 5.9 keV from all detector pixels combined (a and b) and noise spectra of individual pixels (c and d) of the FM SXS. (a and c) without VIS installed; (b and d) with VIS installed. The data were taken before the SXS dewar was installed on the spacecraft.
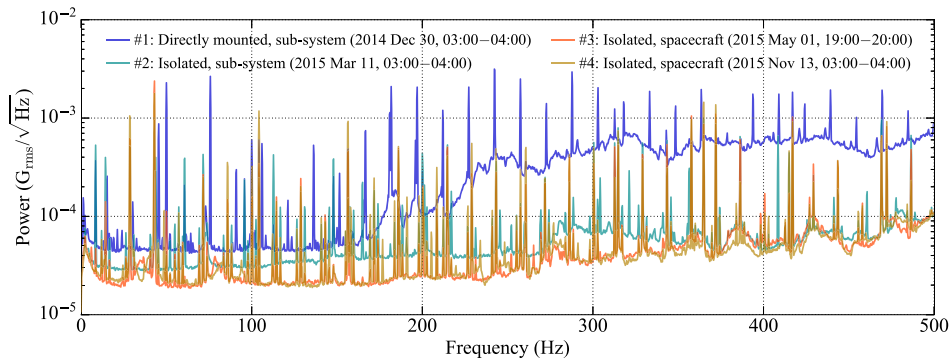
Fig. 8 Acceleration spectrum measured on the FM dewar (at $-Y$ direction on the middle shell), when cryocoolers are in operation. Four curves are for different dewar configurations. Blue (#1): without VIS, before installation of the dewar on the spacecraft; light blue (#2): with VIS, before installation of the dewar on the spacecraft; orange (#3) and brown (#4): with VIS, dewar on the spacecraft, with two different dates (May 01, 2015 and November 13, 2015).

5.3 SXS Performance Across and After the Launch

The spacecraft was launched on February 17, 2016, by the H-IIA rocket from JAXA Tanegashima Space Center. The temperature of the VIS at launch was successfully controlled within the required range (10°C to 25°C).[17] The performance of the cryocoolers in-orbit was consistent with prediction,[8,18] showing that the bumpers successfully worked to prevent excessive mechanical load on the compressors. The energy resolution of the detector in-orbit with all pixel data combined was better than 5 eV at 5.9 keV,[16] indicating no degradation by cryocooler disturbance, i.e., success of the VIS as a vibration isolator. The SXS

including the VIS had operated fine, with no anomaly, until the end of observation on March 26, 2016.

6 Lessons Learned

The disturbance issue of the SXS cryocoolers and the selected mitigation, the VIS, were described. The VIS with bumpers was eventually adopted as a most feasible solution to realize both small transmissibility at high frequency and small acceleration and displacement against vibration during launch and ground testing. The VIS successfully satisfied both requirements leading to successful detector performance in orbit. The use of

bumpers, however, resulted in extremely nonlinear response, making the design and verification quite difficult. Lessons learned from the SXS VIS program are listed below.

6.1 Identifying Critical Issues in Early Phase

Identifying possible critical issues and finding problems in early phase is important. A big design change in the latter stage of the spacecraft development is challenging, because the available design space is small. For this purpose, careful investigation of a possible physical mechanism is essential. Indeed, the micro-disturbance issue had been evaluated in the early stage of the Astro-H development by comparing the expected acceleration to a prior program using a cryocooler and a microcalorimeter (XRS onboard Suzaku satellite[19]). At that time, however, the strong dependence on the frequency of the acceleration was not recognized. As a result, only the absolute value of acceleration was evaluated to underestimate the influence.

The issue might be noticed earlier if more comprehensive component-level tests had been performed, e.g., measurement of susceptibility, along with frequency dependence, of the detector to the vibration. Identifying the physical mechanism is again mandatory to have an appropriate test plan and test apparatus. Once the physical mechanism is understood executing appropriate component-level tests, especially using a breadboard or EM, is a good mitigation to identify the problem early, to avoid late change of the flight design.

6.2 Importance of Verifiability

Verifiability is important. For example, if a launch lock could be used as an alternative to bumpers (i.e., if there were enough available volume to accommodate a launch lock), it would have a significant benefit because the VIS response becomes linear and more predictable. If multiple choices are available, verifiability should be considered in the trade study.

6.3 Importance of Comprehensive Test-Based Verification

For a nonlinear system, such as bumpers, measurements by tests are essential for verification. The tests performed for SXS VIS were mandatory and quite fruitful. Measuring material properties, including temperature dependence, was necessary to finalize the design. Without more than 100 vibrations using the VIS EDU, the maximum possible acceleration at the compressor could not be convincingly estimated, and hence, the verification could not be finished. A positive lesson is that an appropriate test-basis program is applicable for verification of even such a nonlinear system.

6.4 Putting Efforts to Define a Complete and Quantitative Specification

A challenge of the development of the VIS was to satisfy the requirements somewhat conflicting each other. Another even bigger challenge was to make a complete and quantitative set of requirements. It should be emphasized, however, that studies and tests are crucial and worth putting efforts toward to define a complete and quantitative set of requirements, before starting the hardware design.

When the microvibration disturbance issue was identified, the mechanism and hence the allowable vibration level was not clear. Various tests and associated analyses were required

to reach the understanding shown in Sec. 3.2. The test plans were revised and refined to reflect knowledge obtained in the preceding tests. In parallel to these activities, initial trade-off of possible designs was performed. Once we decide to use VIS as a solution, further tests were performed to quantitatively define the allowable level. The design of the VIS shown in Sec. 4.2 occurred after that.

Although this process may take long (10 months for Astro-H), particularly when we encounter an unexpected issue, omitting or reducing efforts on the process would introduce a significant risk that the constructed hardware will not eventually show valid performance. Even though starting design and fabrication with requirements including many assumptions may seem preferable under a tight schedule pressure, it is not recommended.

References

1. R. L. Kelley et al., "The Astro-H high resolution soft x-ray spectrometer," *Proc. SPIE* **9905**, 99050V (2016).
2. T. Takahashi et al., "The ASTRO-H (Hitomi) x-ray astronomy satellite," *Proc. SPIE* **9905**, 99050U (2016).
3. Y. Soong et al., "ASTRO-H soft x-ray telescope (SXT)," *Proc. SPIE* **9144**, 914428 (2014).
4. L. Ravera et al., "The x-ray integral field unit (X-IFU) for Athena," *Proc. SPIE* **9144**, 91442L (2014).
5. W. Jellema et al., "Safari: instrument design of the far-infrared imaging spectrometer for spica," *Proc. SPIE* **10563**, 105631K (2017).
6. T. Matsumura et al., "Mission design of LiteBIRD," *J. Low Temp. Phys.* **176**(5–6), 733–740 (2014).
7. S. Yoshida et al., "Flight model performance test results of a helium dewar for the soft x-ray spectrometer onboard ASTRO-H," *Cryogenics* **74**, 10–16 (2016).
8. R. Fujimoto et al., "Performance of the helium dewar and cryocoolers of ASTRO-H SXS," *Proc. SPIE* **9905**, 99053S (2016).
9. C. A. Kilbourne et al., "The design, implementation, and performance of the ASTRO-H SXS calorimeter array and anti-coincidence detector," *Proc. SPIE* **9905**, 99053L (2016).
10. M. P. Chiao et al., "System design and implementation of the detector assembly for the ASTRO-H soft x-ray spectrometer," *Proc. SPIE* **9905**, 99053M (2016).
11. Y. Sato et al., "Development status of the mechanical cryocoolers for the soft x-ray spectrometer on board Astro-H," *Cryogenics* **64**, 182–188 (2014).
12. N. Iwata et al., "Thermal control system of x-ray astronomy satellite Astro-H: current development status and prospects," in *44th Int. Conf. on Environmental Systems* (2014).
13. S. Yasuda and K. Ishimura, "Method of determining specification for transmissibility of vibration isolator for ASTRO-H soft x-ray spectrometer (SXS)," in *Proc. of the 13th European Conf. on Spacecraft Structures, Materials & Environmental Testing*, Vol. 724, p. 24 (2014).
14. J. Howat et al., "Dual stage isolation-a passive bi-linear application for launch load attenuation and on-orbit jitter mitigation," in *Proc. of ESMATS 2017*, p. 25 (2017).
15. B. Allen et al., "Ground based test verification of a nonlinear vibration isolation system for cryocoolers of the soft x-ray spectrometer (SXS)

onboard ASTRO-H (Hitomi)," in *IEEE Aerospace Conf.*, pp. 1–8 (2017).

16. F. S. Porter et al., "In-flight performance of the soft x-ray spectrometer detector system on ASTRO-H," *Proc. SPIE* **9905**, 99050W (2016).

17. N. Iwata et al., "Evaluation of in-orbit thermal performance of x-ray astronomy satellite 'Hitomi'," *J. Spacecr. Rockets* **55**(1), 77–84 (2017).

18. M. Tsujimoto et al., "In-orbit operation of the ASTRO-H SXS," *Proc. SPIE* **9905**, 99050Y (2016).

19. R. L. Kelley et al., "The Suzaku high resolution x-ray spectrometer," *Publ. Astron. Soc. Jpn.* **59**, S77–S112 (2007).

20. Y. Takei et al., "Vibration isolation system for cryocoolers of soft x-ray spectrometer (SXS) onboard ASTRO-H (Hitomi)," *Proc. SPIE* **9905**, 99050X (2016).

Yoh Takei is an associate senior researcher at Japan Aerospace Exploration Agency. He received his BS, MS, and PhD degrees in physics from University of Tokyo in 2001, 2003, and 2006, respectively. His current research interests include cryogenic detectors and systems engineering.

Biographies for the other authors are not available.